Environmental Earth Sciences (2026) 85:204
https://doi.org/10.1007/s12665-026-12935-z

ORIGINAL ARTICLE

Permeability evolution of claystones and other sealing materials for CO_2 storage: role of confining stress and time

Dorina Juhász[1] · Benjamin Busch[1] · Chaojie Cheng[1] · Christoph Hilgers[1]

Received: 10 October 2025 / Accepted: 21 March 2026

Abstract
Carbon Capture and Storage (CCS) is a promising approach that has been increasingly utilized for reducing atmospheric carbon dioxide (CO_2) levels. The long-term security of CO_2 sequestration in saline aquifers depends on the integrity of overlying sealing units, while the transmissive properties of multi-barrier sealing systems remain to be further elaborated. This study investigates the permeability of claystones and compares them with other low-permeability lithologies (evaporites, tight sandstones, and tight limestones, $1 \times 10^{-17} - 1 \times 10^{-21}$ m² at 30 MPa) as well as casing cements ($1 \times 10^{-16} - 1 \times 10^{-22}$ m² at 30 MPa) under CO_2 storage conditions. Permeability was measured using helium gas and, for selected samples, with CO_2. The stress-sensitivity of Klinkenberg-corrected permeability was assessed under confining pressures of 10–30 MPa, and pressure sensitivity coefficients (γ-values) were determined. Time-dependent effects were evaluated by maintaining samples at 30 MPa (approximately 2 km depth of effective pressure) confining pressure for 5–8 days. Results indicate that claystones reduce permeability by approximately one order of magnitude after 3–5 days, while casing cements decrease permeability by two orders of magnitude in 3 days. These findings highlight the necessity of allowing caprock samples to equilibrate under targeted effective stresses for at least three days to obtain reliable permeability measurements. Furthermore, our measured permeability varies distinctly across lithotypes (shales, evaporites, tight sandstones, and tight limestones), spanning 2 to 6 orders of magnitude at low confining stresses, necessitating the site- and lithotype-specific assessment of sealing unit permeability.

Keywords Claystone · Gas-permeability · Stress-dependency · Heterogeneity · CO_2 storage · Casing cement

Introduction

While global CO_2 emissions are increasing, the installation of wind- and hydropower, as well as photovoltaics and geothermal, among others, leads to decreasing CO_2 emissions in 23 countries, including the European Union and the United States of America (Friedlingstein et al. 2023, 2025). However, according to IPCC (2023), the climate target is not achievable without using carbon capture and storage (CCS), especially for hard-to-abate emissions (e.g. concrete manufacturing) (Hilgers and Schilling 2024). Therefore, studying the possibilities of CCS has become an important research topic over the past decades (Abraham-A et al. 2024; Alcalde et al. 2018; Atef et al. 2025; Budinis et al. 2018; Chadwick et al. 2008).

For the geological CO_2 storage reservoir system in saline aquifers, a cap rock is important to avoid leakage. Permeability is a critical property in reservoir geology and in the assessment of the capacity of sealing rocks (Zhao et al. 2024). To determine the gas permeability, particularly for low-permeability systems, the Klinkenberg correction has to be used due to the gas-slippage effect (Klinkenberg 1941). Although caprock properties have been extensively studied over the past decades, sedimentary rocks, like claystones, exhibit lateral heterogeneity in their mineralogical and petrophysical properties (Chandler et al., 1989; Schmidt et al., 2020). As a result, site-specific analysis of caprocks remains essential to assess the multi-barrier complex, while applications of this technique in depleted hydrocarbon reservoirs, with proven cap rock integrity may not strictly necessitate these analyses. Permeability within a single rock type can

✉ Dorina Juhász
dorina.juhasz@kit.edu

[1] Institute of Applied Geosciences – Structural Geology and Tectonics, Karlsruhe Institute of Technology, Adenauerring 20a, Karlsruhe 76131, Germany

Published online: 10 April 2026

exhibit considerable variation due to different pore-size distribution, grain-size distributions, clay mineral content and general mineral assemblage (Carcione et al. 2019; Ecay et al. 2020). Yang et al. (2017) demonstrated that, within the same formation, porosity can range between 1.5 and 7.3%, while permeability may vary by up to 4 orders of magnitude in tight gas reservoirs. Such variability is not limited to reservoir rocks, it can also occur in potential caprocks (Febbo et al. 2025). Shales are often considered suitable caprocks due to their inherently low permeability (Neuzil 2019). However, variations in silt and clay contents can still lead to heterogeneity in both permeability and porosity (Molenaar et al. 2007).

Several studies report reduced permeability under increasing confining pressure, due to pore collapse or microfracture closing in case of silt- and sandstones (Alam et al. 2014; Chen et al. 2002; Kozhevnikov et al. 2021; Wong et al. 2013). They often omit the duration for which samples were subjected to confining stresses prior to permeability measurements. Other studies show that permeability at the same confining stress can change over time due to deformation, dissolution, and creep (Bandara et al. 2021; Chen et al. 2022; Zhu et al. 2024). However, these studies focus on fracture permeability only, assuming the rock matrix is impermeable. Therefore, in this study, we focus on the overall permeability change over time to close this gap in the application to potential cap rocks for CCS in Germany.

David et al. (1994) derived an equation to calculate the pressure-permeability sensitivity (γ -value) of rocks. γ -values were used to explore links between the pressure sensitivity, time-dependent permeability, and different lithotypes. To prevent permeability changes during injection, it is essential to understand the rate of permeability variation over time and pressure change in relation to lithology. These stress hysteresis measurements can highlight if the permeability follows different paths during the loading and unloading cycles, and prevent formation damage caused by fluid injection and cyclic loading. This method also allows to correct for uplift induced fractures (Teklu et al. 2016).

In this study, we focus on the characterization of low-permeable rocks, including typical sealing lithologies such as claystones and evaporites, but also assess tight sandstones, limestones, and casing-casing cement. These materials are key to both stratigraphic trapping and capillary trapping mechanisms (Massarweh and Abushaikha 2024). We selected individual claystones and evaporites (ranging from intraformational caprocks interbedded with reservoir rocks to extra-formational cap rocks) and compared them to other low-permeability rocks, including three tight sandstone samples, and one tight limestone sample. The tight limestone was chosen as it is already acting as a sealing lithology toward rising mine water levels in a former coal mining area (Ölmez et al. 2024; Quandt et al. 2022) and may be a potential barrier lithology in other parts of the North German Basin. The tight sandstones were chosen to assess the potential reservoir lithology capped by intraformational shales (Greve et al. 2024b) and highlight mineralogical and granulometric influences on stress-dependent permeability. Casing cement is an important barrier required to prevent CO_2 leakage; therefore, we study and compare them here in relation to natural cap rocks (Gan et al. 2025). The resulting data support informed, data-driven discussions on CO_2 storage in Germany and offer insights applicable to similar studies worldwide. In particular, the observed effects of prolonged exposure to elevated confining pressure (30 MPa) on permeability provide valuable guidance. This work also demonstrates how lithological heterogeneity, even among different claystones and in low-permeability rocks from Germany, affects petrophysical properties, emphasizing the need for site-specific assessments.

Geological background and samples

The measured samples belong to Upper Carboniferous, Upper Permian, Lower Triassic and Upper Cretaceous sedimentary and evaporite sequences deposited in Northwest Germany (Fig. 1).

The Upper Carboniferous clastic sediment samples originate from the foreland basin of the Variscan orogen, Northwest Germany, which was deformed after the Westphalian (Drozdzewski 1993). These sediments are deposited on the coastal plain and in a deltaic environment (Fig. 1) (Greve et al. 2023; Muller and Steingrobe 1991). The samples are from two different boreholes, Frenzer Staffel-1 (UC_4, UC_5 and UC_6, Fig. 2) and Haidberg-1 (UC_2, Fig. 2). The Frenzer Staffel-1 borehole is located in the southwestern part of the basin, in the Inde Syncline, while the Haidberg-1 well is located in the Ruhr Basin (Greve et al. 2024a). Based on the coal seams in the cores of well Frenzer Staffel-1, tight sandstones belong to the Westphalian A and B (Wrede and Zeller 1991), while the black shale samples of well Haidberg-1 belong to the Westphalian B Horst Formation (Fm.). The Upper Carboniferous shales are intraformational seals to the intercalated, mostly fractured, tight sandstone samples. The total thickness of Westphalian A and B can reach up to 2000 m in the Ruhr Basin (Doornenbal and Stevenson 2010). The UC_2, UC_5, and UC_6 samples are from the core material, while UC_4 is from an outcrop.

The Upper Permian Zechstein evaporitic sequence (Fig. 1), deposited in closed lagoons after multiple transgressional cycles in the North German Basin (Meschede 2018), acts as a major cap rock lithology in Northern Europe (Strozyk et al., 2017). In the Zechstein, seven

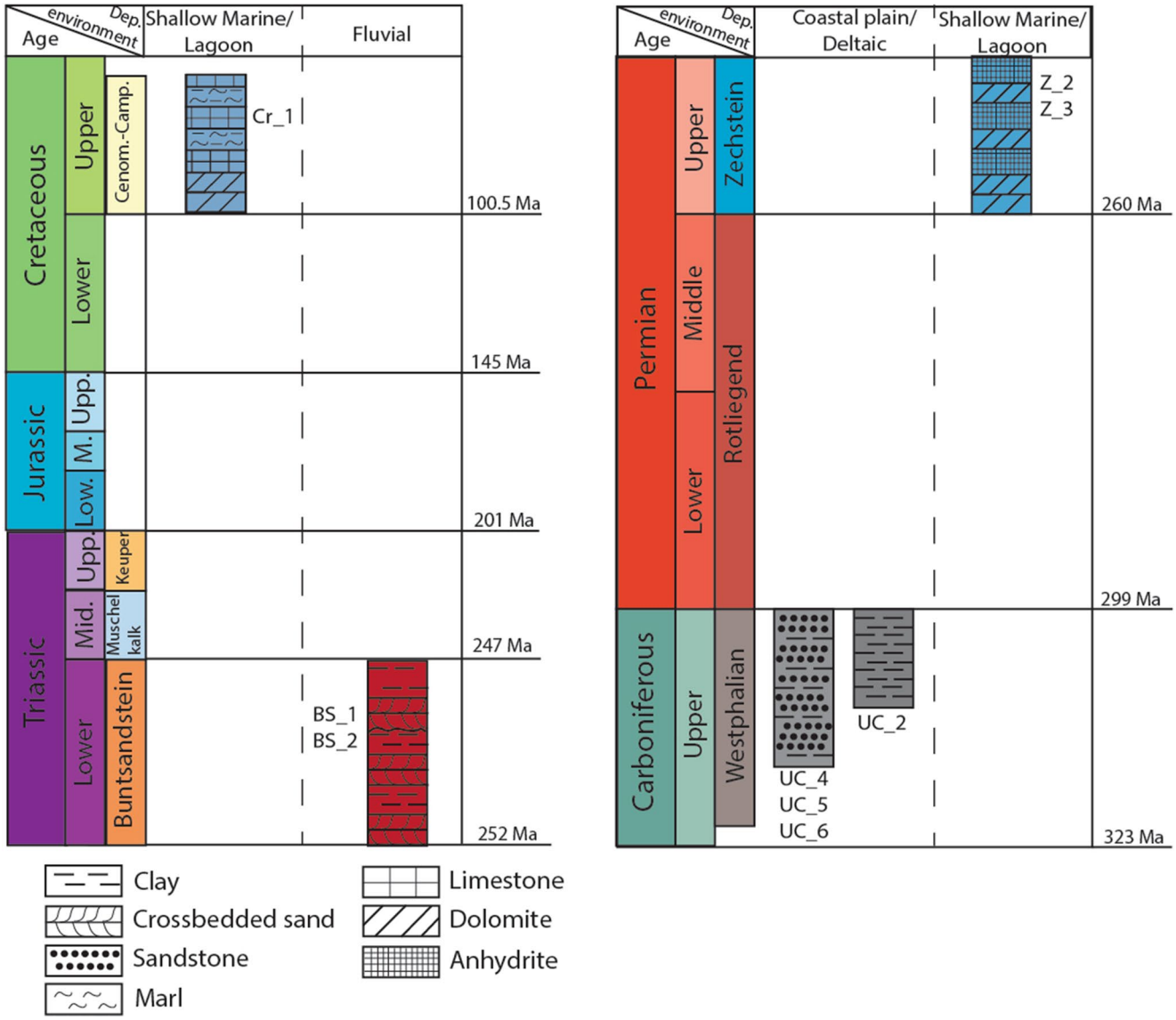

Fig. 1 Simplified stratigraphic column of the measured samples. UC – Upper Carboniferous, Z – Zechstein, BS – Buntsandstein, Cr – Upper Cretaceous

transgressional cycles can be distinguished, where the contents of anhydrites, carbonates, and salts vary (Menning et al. 2011). The carbonates can be found mostly on the rims of these lagoons, while the anhydrites are present in the center (Meschede 2018). The Zechstein evaporites are acting as effective seals to underlying natural gas reservoirs in the Southern Permian Basin, highlighting their capacity as seals. The thickness of the Zechstein may vary between 200 and 1800 m in Northern Germany (Doornenbal and Stevenson 2010). In this study, five samples (BS_1, BS_2, UC_2, Z_2, and Z_3, Fig. 2) were retrieved from core material from Northwestern Germany.

The Lower Triassic Buntsandstein in northern Germany can be subdivided into three general groups based on (Boigk 1959): (1) the fine-grained, oolitic Lower Buntsandstein; (2) the fine- to coarse-grained Middle Buntsandstein containing shales; and (3) the pelitic Upper Buntsandstein interbedded by evaporites. The Middle Buntsandstein comprises the Volpriehausen and Hardegsen formations, both showing an upwards-fining cyclicity, that starts with medium-, or coarse-grained sandstone and ends with pelitic sediments, deposited in fluvial-lacustrine environments (Fig. 1) (Filomena and Stollhofen 2011; Geluk and Röhling 1997; Szurlies 2004). These cycles can be correlated with drier and wetter periods caused by Milankovitch cycles (Szurlies 2004). The maximum thickness of the Middle Buntsandstein may reach 2500 m in Northern Germany (Doornenbal and Stevenson 2010). Here, two samples from the intraformational red shales of the Middle Buntsandstein (BS_1 and BS_2) are studied. The samples are from the upper part of these

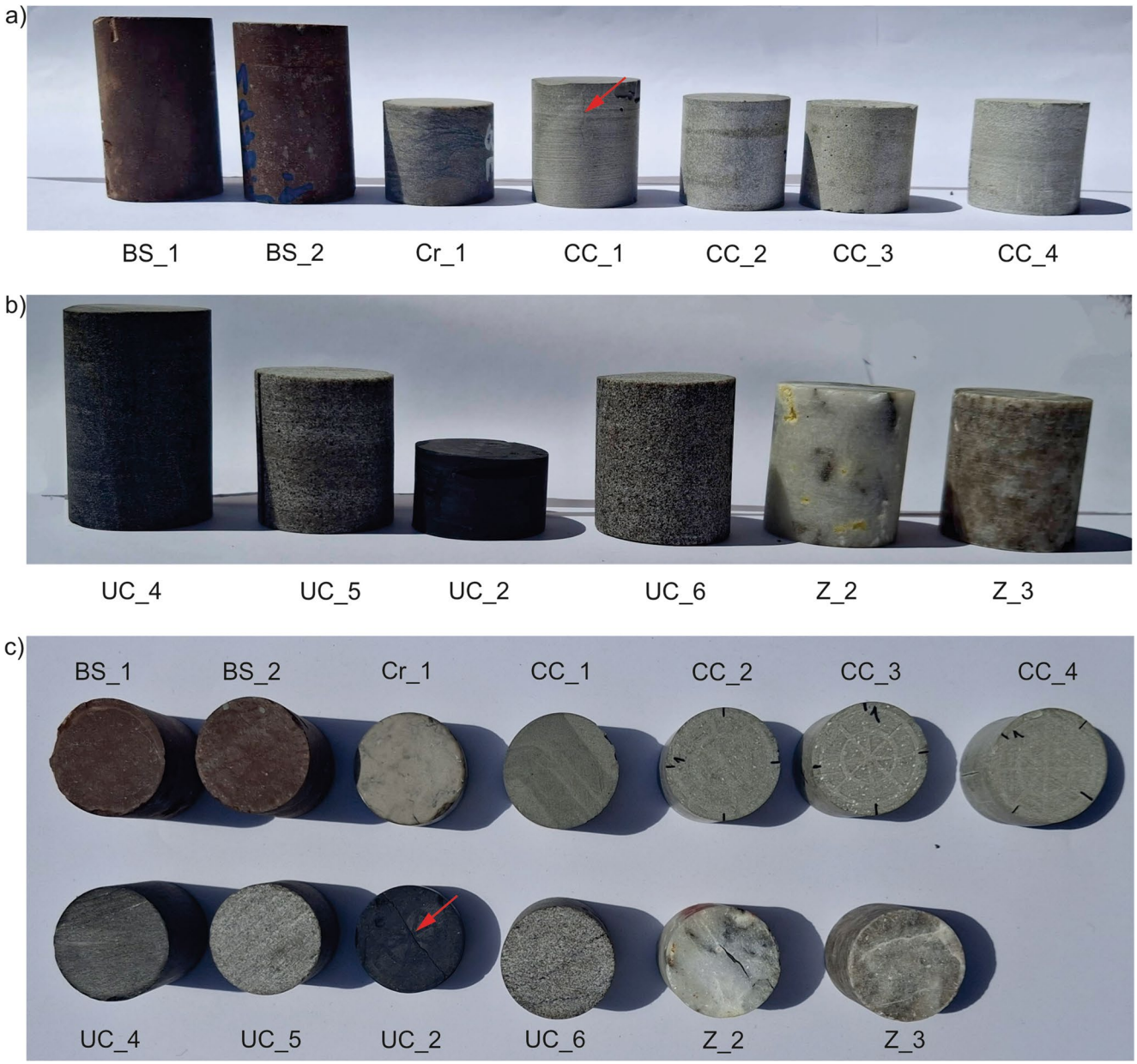

Fig. 2 Plate of the used plug samples. (**a**) Buntsandstein, Cretaceous carbonate and casing cement samples, (**b**) Upper Carboniferous and Zechstein samples. (**c**) All of the samples from above. The fracture in the sample UC_2 developed during the measurements. The red arrows indicating the macrofractures in the sample. In case of CC_1 it was already a preexisting fracture, while at UC_2 it developed during measurement

cycles and are retrieved from core material from Northwestern Germany.

Upper Cretaceous (Campanian) carbonates were deposited in the Central Münsterland Cretaceous Basin, Northwestern Germany (Ölmez et al. 2024). The Münsterland Basin is represented as the southern marginal trough of the inverted Lower Saxony Basin (Voigt et al. 2021). These shallow marine basin sediments are deposited on the shelf-margin to slope environment (Ölmez et al. 2024), reaching a total thickness of 2000 m (Scheck-Wenderoth et al. 2008). The studied samples belong to the Upper Campanian Beckum Member (Ahlen Fm.), which is built up by alternating limestone-marly shale sequences and has a thickness of 25 m (Fig. 1) (Giers 1958).

The CC_1 casing cement was provided by Technical Petrophysics (AGW-TP) at KIT and is a pure cement with a water-cement (w/c-ratio) ratio of 0.44 and is classified as a Class G well cement. The other casing cement samples (CC_2, CC_3 and CC_4, Fig. 2) were provided by the Institute of Concrete Structures and Building Materials (IMB) at KIT, and contain

20 m% dry polymer (Bruckschlögl et al. 2026). The polymer in CC_2 is Styrene-acrylic ester (SAE), in CC_3 is Styrene-Butadiene (SB), and in CC_4 is Ethylene-Vinyl Acetate (EVA). These samples were also made from Class G cement, having a w/c-ratio of 0.44. CC_1 has shown a macroscopic crack, while CC_2 and CC_3 cracked due to drying (1–5 µm crack) and in CC_4 no cracks were detected during optical inspection.

Materials and methods

Five different lithologies, among them two different claystones, and two different types of casing cement, providing a total of 13 cylindrical plug samples with a 1-inch (~2.54 cm) diameter, were used for this study. The rock samples are from boreholes as well as from outcrops (Supplementary materials 1). Although the lengths of the samples vary, according to (Heap 2019), samples with a 25 mm diameter and with small pore sizes, as in our samples, the permeability measurements will not be affected by the length of the sample. The natural rock samples were dried in a vacuum oven at 40 °C for four days, the CC_2, CC_3, and CC_4 dried in a climate room at 20 °C and 65% relative humidity (Bruckschlögl et al. 2026).

Porosity

Porosity was determined using a semi-automated helium pycnometer, AccuPyc II 1340 by micromeritics (Greve et al. 2024a). Based on the measured solid volume and determined bulk cylinder volume, the porosity can be calculated. The porosity results are given in percentage (%) and the accuracy is specified as 0.045% of the porosity value.

Mercury intrusion capillary pressure (MICP) measurements were carried out for 3 samples showing deviating gradients during Klinkenberg-correction using a micrometrics AutoPore IV 9520 (pore throat size: 360–0.003 µm). This method allows the calculation of the pore throat size distribution within the sample (Knopp et al. 2022).

Gas permeability

No universal measurement standards have been developed for ultra-low gas permeability measurements (Sander et al. 2017). Darcy's law and the Klinkenberg effect are the most widely used applications to interpret low permeability measurements (Sander et al. 2017). The permeability values were measured using the steady-state flow-through method in an isostatic flow cell (Becker et al. 2019), using single-phase gas flow with helium and CO_2 as permeants. A high-performance liquid chromatography (HPLC) pump was used to generate hydrostatic confining pressure using water on the cylindrical plug sample encased in a heat-shrinking sleeve (Fig. 3). The studied plugs were measured at 10, 20, and 30 MPa confining pressures, respectively. The apparent permeability values were Klinkenberg-corrected (Klinkenberg 1941). For the Klinkenberg correction, the samples were measured with different inlet pressures at each confining pressure, ranging between 2.5 and 4.7 MPa. The apparent permeability was measured at least with 3 different inlet pressures, up to 10 times. To calculate the gas permeability, the following equation was used;

$$K_a = K(1 + \frac{b}{p}) \quad (1)$$

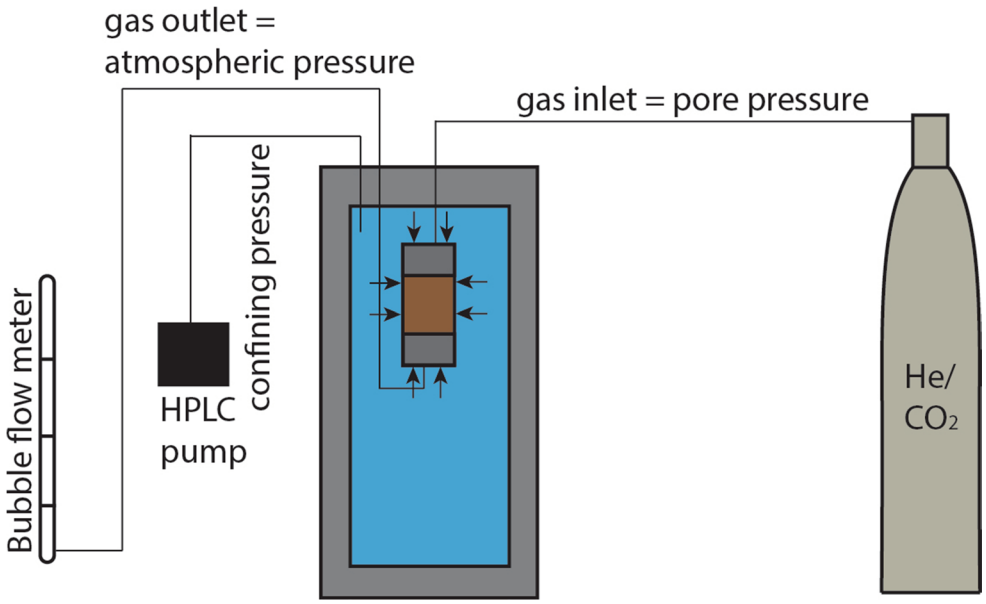

Fig. 3 Flow-through measurement setup for gas permeability measurements. HPLC stands for high pressure liquid chromatography

where K_a is the apparent permeability, K is the intrinsic permeability, b is the slippage factor, and p is the mean of the inlet and outlet pressures. To calculate the value of the measurement errors, the standard deviation of a series of measurements was determined. Based on the value of standard deviation, the standard error was calculated, which is 1.5% of the given permeability measurements. The standard error was calculated based on several measurements of anhydrite samples at 10 MPa confining pressure. The standard deviation of the measured Klinkenberg-corrected data was calculated, then the standard deviation was divided by the square root of the number of measurements.

Stress-dependent permeability

Stress sensitivity describes permeability changes as a function of confining stress changes (MPa^{-1}), allowing to evaluate how sample compaction affects permeability (David et al. 1994). To assess the stress sensitivity of the studied samples, we derived the γ-value based on the exponential law (Eq. 2) (David et al. 1994) for permeability measurements with varying confining stresses.

$$\mathrm{K} = \mathrm{K}_0 \exp\left[-\gamma\left(\mathrm{P}_e - \mathrm{P}_0\right)\right] \quad (2)$$

where K is the permeability under the effective confining pressure P_e, K_0 is the permeability at reference effective pressure P_0, and γ is a constant. A higher γ-value means a higher compaction-induced permeability reduction. The exponential law was mostly studied for samples with porosity between 14 and 35% (David et al. 1994; Dong et al. 2010), but in our case, all the samples are below this range.

Additionally, stress hysteresis measurements were performed with four loading-unloading cycles to determine the irreversible permeability changes in a sample. In the loading half-cycles permeability was measured at 10 MPa, then 20 MPa and finally at 30 MPa confining pressure within one day. Afterwards, the sample was left at 30 MPa confining pressure overnight and the next day the permeability was measured at 30 MPa, then at 20 MPa and finally at 10 MPa confining pressures for the unloading half-cycle. Over the following night the sample stayed under 10 MPa confining pressure. These cycles were repeated four times.

Time-dependent permeability

To assess time effects under elevated confining stresses (30 MPa), we conducted time-series measurements and compared the results across lithologies. Four samples (BS_2, UC_2, Z_3, CC_2) were measured once daily for five to eight days at constant confining pressure of 30 MPa to quantify time-dependent permeability variation.

Gas type effects on permeability measurements

Three samples (BS_1, CC_3, Z_2) were measured using carbon dioxide and helium as permeants to assess the influence of gases with different molecular sizes on permeability. With both gases the permeability was measured at different confining stresses and inlet pressures (2.5 ± 0.2 MPa, 3.5 ± 0.2 MPa, and 4.5 ± 0.2 MPa).

Results

Porosity and permeability (at 30 MPa confining stress)

The porosity of the measured samples ranges between 1 and 14%. Klinkenberg-corrected permeability at 30 MPa confining stress of the studied samples ranges from 10^{-16} to 10^{-22} m² (Fig. 4, Supplementary materials). The studied samples do not show a positive correlation between the two properties (Fig. 4), but a clear positive trend can be recognized among the silty sandstone samples, however the claystone samples show variability. The same rock types within the same lithology show some differences in porosity and permeability values (e.g., BS_1 and BS_2, UC_4, UC_5 and UC_6, Z_2 and Z_3). The black and red claystones cover a permeability range of two orders of magnitude (10^{-21} – 10^{-19} m^2), tight sandstones cover three orders of magnitude ($10^{-21} - 10^{-18}$ m^2), anhydrite covers one order of magnitude ($10^{-18} - 10^{-17}$ m^2), and casing cement samples of different composition cover six orders of magnitude ($10^{-22} - 10^{-16}$ m^2). Individual tight silty sandstones (UC_4) even have lower permeability values than a shale sample (UC_2) from the same formation.

Pore size distribution and mercury porosity

Based on the MICP measurements, the median pore throat radius of sample BS_1 is 5.22 nm, of UC_2 is 3.97 nm, and of Z_2 is 14.98 nm. Pore throat radii are thus mostly smaller than 10 nm. Sample Z_2 generally shows a larger pore radius than BS_1 and UC_2, but this sample contains druses (Fig. 2). According to Bruckschlögl et al. (2026) the pore size distribution of the casing cement samples (CC_2, CC_3, and CC_4) is mainly smaller than 100 nm (Fig. 5).

Stress-dependent permeability

With increasing confining stresses, permeability decreases, except for sample Cr_1, which shows a slight increase (Fig. 6a). Where the permeability decreased at increasing

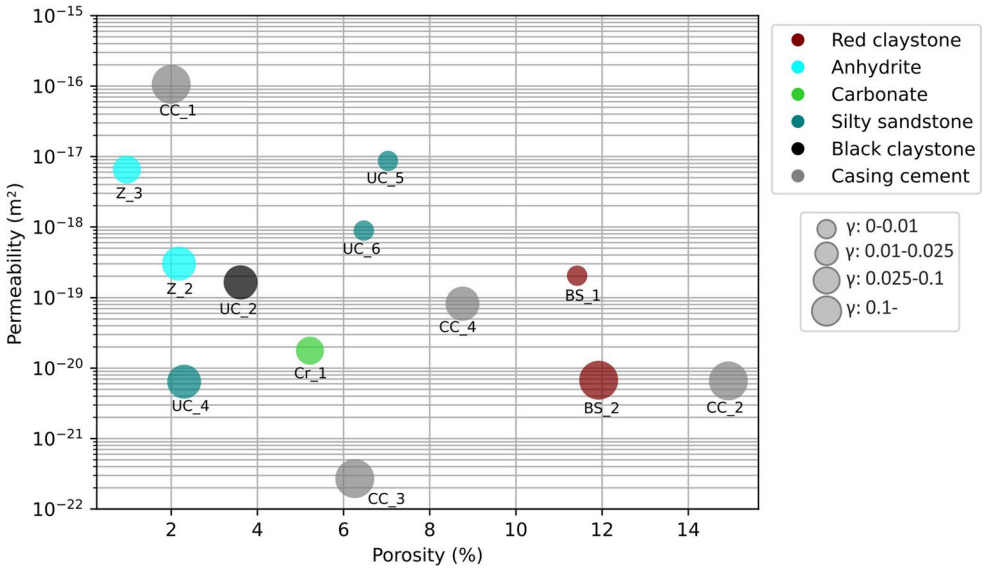

Fig. 4 Porosity – permeability (at 30 MPa confining stress) and pressure sensitivity diagram of the samples. The size of the circles shows the range of the calculated γ-values (Supplementary materials)

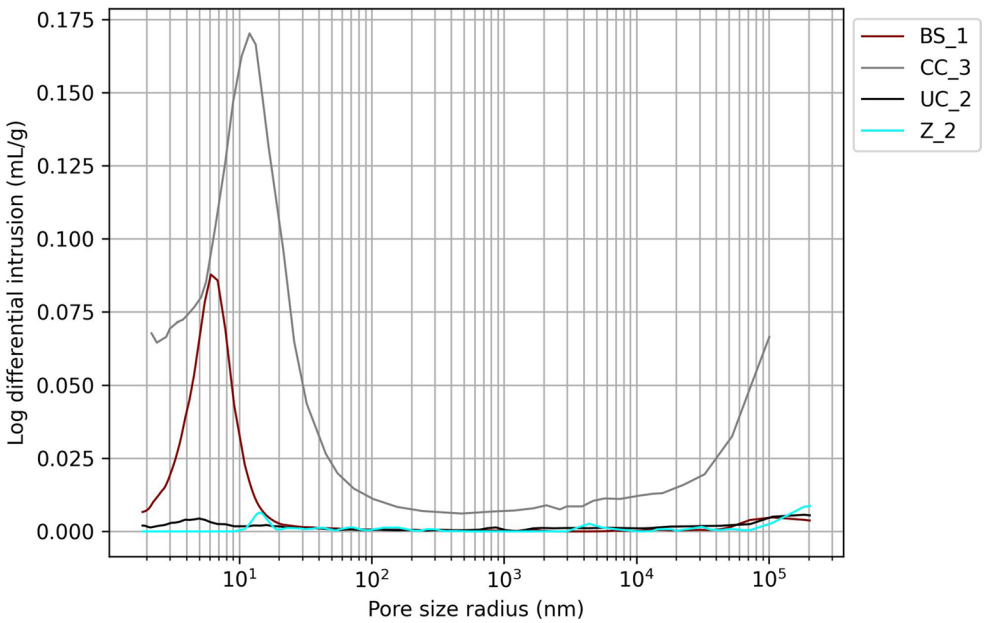

Fig. 5 Pore size distribution of BS_1, CC_3, UC_2 and Z_2 samples determined by MICP. The pore size distribution of CC_3 is after (Bruckschlögl et al. 2026)

confining stresses, the decrease is less than one order of magnitude, except for samples CC_1 and CC_3, which show a larger decrease, in the case of CC_1 from 4.45×10^{-15} m^2 to 1.05×10^{-16} m^2, and CC_3 from 6.8×10^{-20} m^2 to 2.69×10^{-22} m^2. CC_2, CC_3, and CC_4 show ductile deformation with the sample deforming into the gas flow channels of the end plug (Fig. 2). Although BS_1 and BS_2 are both red claystone samples from the same formation, they show a different decreasing trend, which is also reflected by the γ-values. For BS_1 it is 0.009 MPa^{-1}, while for BS_2 is 0.104 MPa^{-1}. Furthermore, the initial permeability values were plotted regarding stress dependency (Fig. 6b), but for CC_4 only apparent permeability could be measured at 10 MPa confining pressure.

A general trend can be discovered, samples from the same lithology with lower permeability have always higher γ-values (Figs. 4 and 6b). For samples, where the permeability only slightly changes with confining pressure (e.g. UC_5, UC_6, Z_3) the fitted exponential curve for γ-values have very low R^2.

The calculated pressure sensitivity of the permeability (γ-values) varies between 0.001 and 0.2 MPa^{-1}. We observed, that samples BS_1, BS_2, Cr_1, UC_5 and UC_6 have γ-values lower than 0.02 MPa^{-1}, while Z_3 is only slightly above 0.02 MPa^{-1} (Fig. 6b, Supplementary materials). The γ-value ranges differ between the different lithotypes (Fig. 7). However, the claystone, silty sandstones, and the single limestone have very similar medians (0.01–0.02

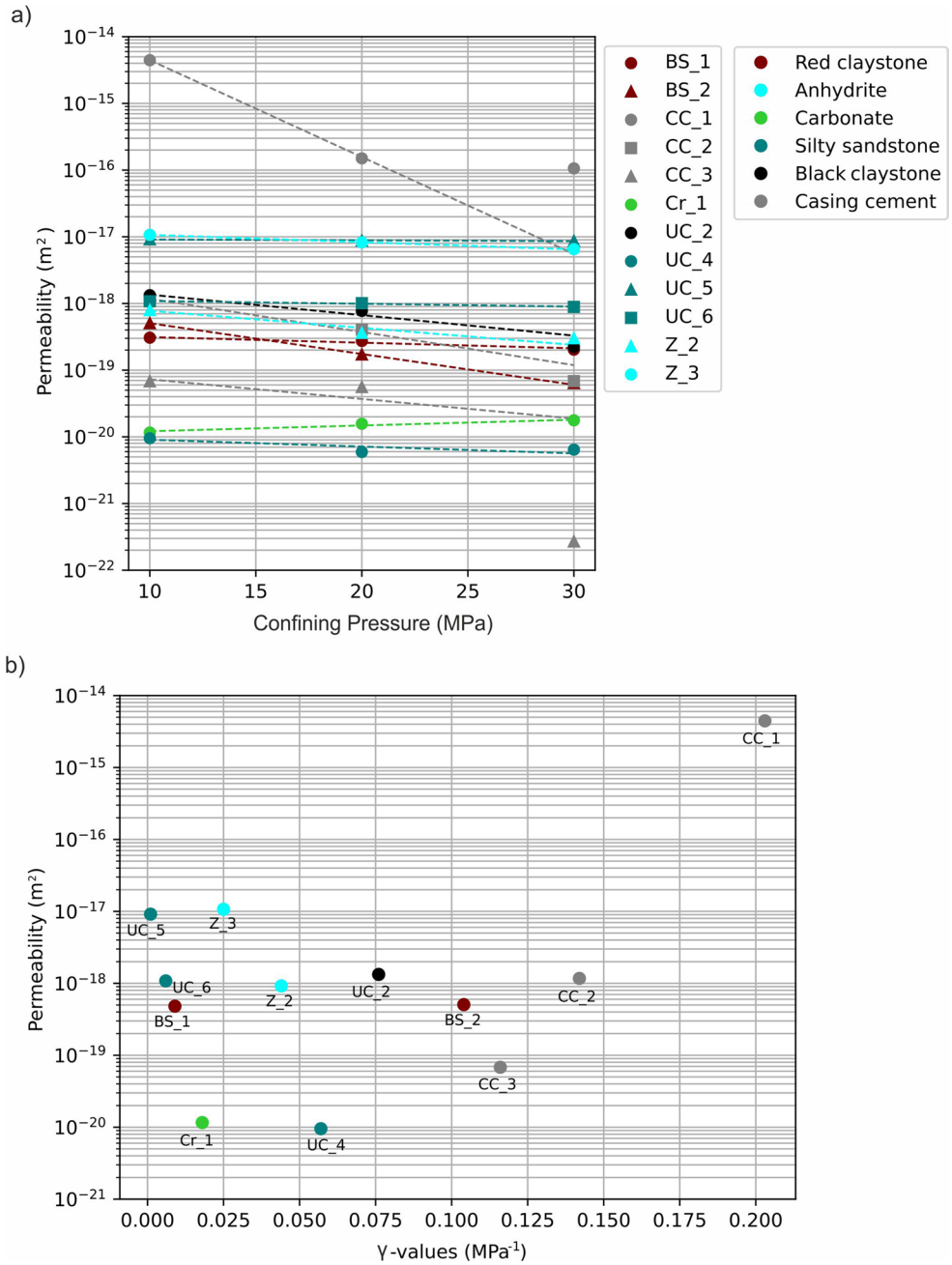

Fig. 6 **(a)** Klinkenberg-corrected permeability values at different confining pressures (10, 20 and 30 MPa). Most of the samples show a reversed trend between confining pressure and permeability. The dashed line is the exponential trendline, where the γ-values are derived from. (**b**) Permeability at 10 MPa confining pressure and corresponding γ -values derived from the permeability values of (a)

MPa^{-1}). The anhydrite samples have a slightly higher median at 0.03 MPa^{-1}. The highest variability among the sealing rocks is shown by claystone samples.

Time-dependent permeability

Permeability variations under elevated confining pressure of 30 MPa cover up to eight days (Fig. 8). No change can be observed over time in the permeability of silty sandstones (UC_5, UC_6) and one of the anhydrite samples (Z_3). BS_2 (red claystone) shows a rapid decrease between the first and second day, then it decreases at a slower rate until it stabilizes on the fourth day. The permeability of UC_2 (black claystone) decreases at the same rate until the third day, then it increases and stabilizes. Z_2 (anhydrite) shows an abrupt decrease in its permeability, after the first day and third day. Sample CC_2 (casing cement) initially shows a permeability decrease by 3 orders of magnitude in the first three days, but from the fourth day, the permeability increases again (Fig. 8a). Cr_1 (limestone) follows a decreasing trend (2 orders of magnitude) until the third day, then the permeability starts to vary. Furthermore, samples CC_2, Cr_1, UC_2, and Z_2, which experience 30 MPa confining pressure for more than 5 days, occasionally show

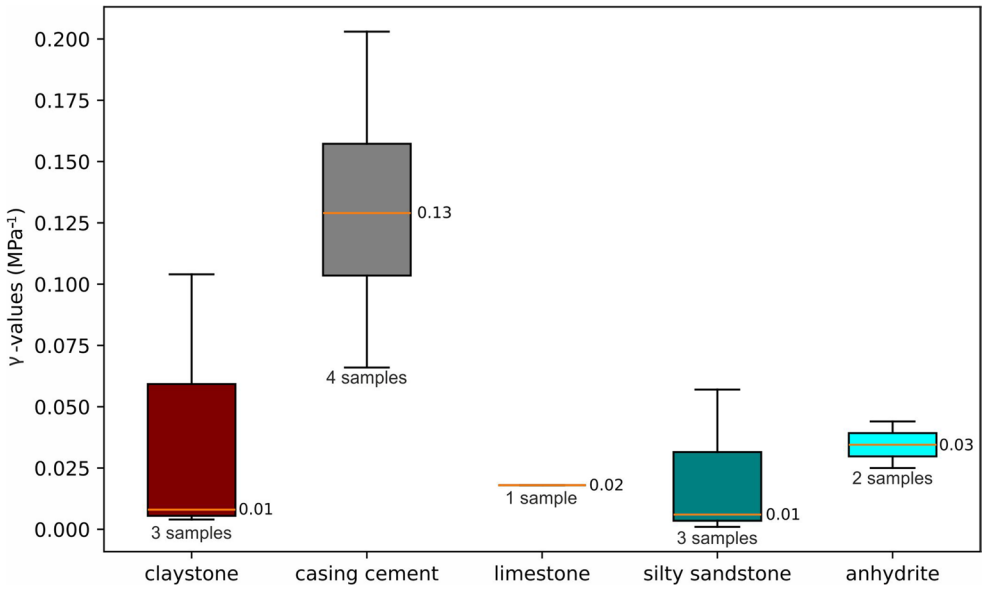

Fig. 7 γ-value distribution in regard to the rock type. The claystone bar includes 3 samples, the casing cement 4, the limestone is only 1, silty sandstone 4, and anhydrite 2 samples

an increase in permeability (Fig. 8a). CC_2 and Cr_1 show a notable increase after the third day, while in the case of UC_2 and Z_2 only a slight increase can be seen. We tried to determine whether there is a correlation between the γ–values and the time required to achieve stable permeability values at 30 MPa confining pressure. Samples, having lower γ-values (UC_5, UC_6, and Z_2), needed less time to achieve stable permeability values (1 day) at 30 MPa confining pressure, than the other samples with higher γ-values (Fig. 8). Samples with γ-values above 0.025 MPa^{-1} required more than one day until measurements were reproducible (Fig. 8b).

Stress hysteresis

Stress hysteresis measurements were performed for claystone sample BS_1 ($\gamma = 0.009$ MPa^{-1}). The initial decrease in permeability during increasing confining stresses (1st loading) is the highest (4.810×10^{-19} to 7.526×10^{-20} m^2), and during subsequent loading and unloading cycles, permeability values at 10 and 20 MPa are always much lower than in the first loading cycle (max. 1.235×10^{-19} m^2, Fig. 9). The loading values in the first and third cycles are higher than the unloading values (Fig. 9). The last unloading cycle also shows higher permeability values than the previous two cycles (Fig. 9). After the first loading cycle, the end members at 10 and 30 MPa confining pressures are generally comparable, but the path during loading and unloading is always different. A large discrepancy is shown in the third (blue) and fourth (yellow) cycles. The permeability was the lowest during the third cycle, afterwards it returned to the values of cycle 1 and 2.

The calculated γ-value changes between the loading and unloading cycles, where during the unloading stages the γ-values are higher than during the loading stages, except for the first cycle. However, it is important to mention, that γ-values for the third and fourth cycle are not trustable values due to their low R^2.

Effect of gas type on permeability measurements

As the samples (BS_1 and Z_2) used for the assessment of the influence of the type of permeant on permeability measurements show median pore-throat sizes < 6 nm (Fig. 5), this section only compares apparent permeabilites, because no slip-flow occurs in these samples due to their pore throat size. The apparent permeability was measured with the same inlet pressures for He and CO_2, therefore it is possible to compare the apparent permeability values. The measured values at each confining pressure and for different inlet pressures can be seen in Table 1 for both gases separately. The CO_2 permeability of BS_1 is one order of magnitude lower than the He-permeability (Table 1). Similarly, in the case of sample CC_3 the CO_2-permeability could not be measured at all, as no gas flow could be initiated, while He-permeability could still be measured (Table 1).

Discussion

Porosity-permeability correlation

An overall correlation between porosity and permeability cannot be determined for this database containing multiple rock types (Fig. 4), while the UC samples by themselves may imply a positive correlation for a subset of samples. This is in agreement with assessments of Bernabé et al. (2003), who stated that nano-porous rock types do not

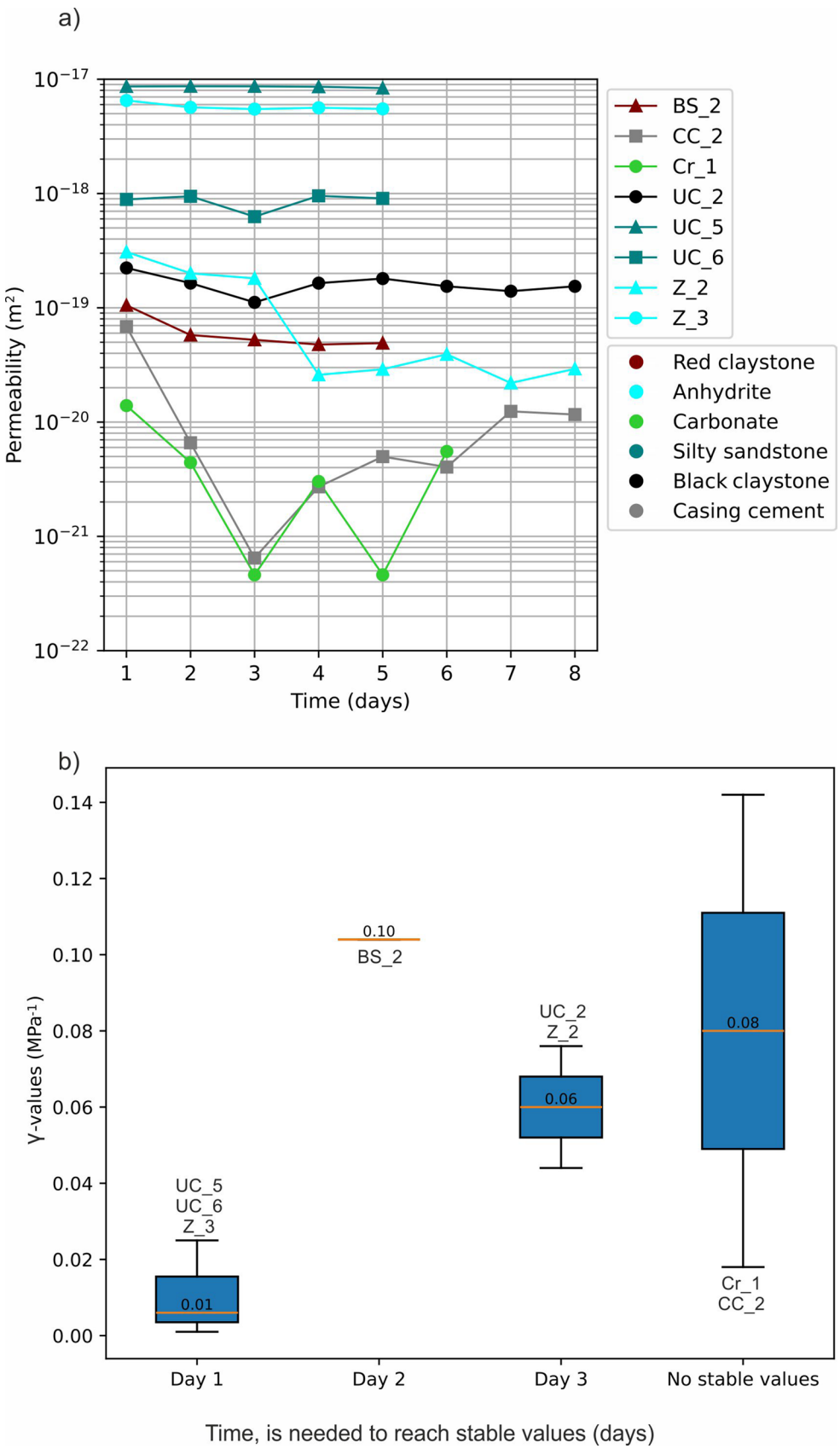

Fig. 8 **(a)** Permeability measurements at 30 MPa confining pressure over several days. Each line shows a different sample with different lithology. **(b)** The average γ-values of different rock indicate how long the samples had to be pressurized to reach stable permeability values

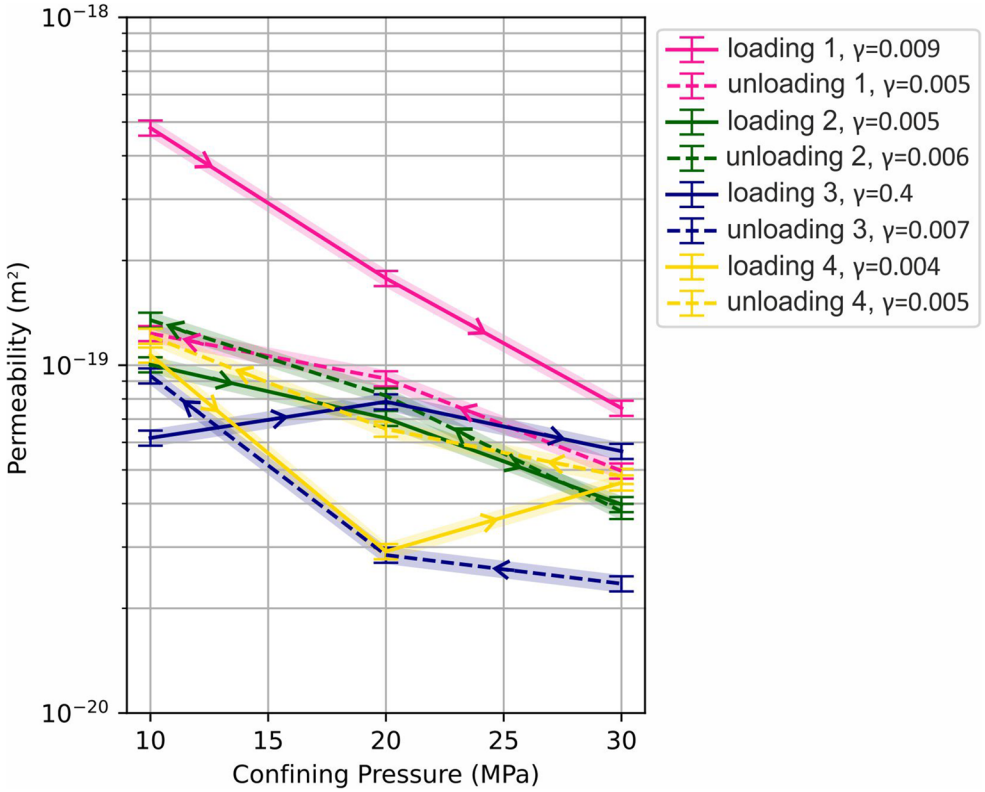

Fig. 9 Loading (solid lines) and unloading (dashed lines) stages during four different cycles (pink, green, blue and yellow), the arrow shows, if the confining pressure decreases or increases. The error is represented by the shaded background show 5% error. Stress hysteresis measurements show that the initial permeabilities of the first loading cycle cannot be matched after the first loading cycle. The calculated γ-values for each stage are shown in the legend

Table 1 Measured permeability values at different confining pressures with different gases. The first column shows the confining pressure (MPa), the second the gas inlet pressure (MPa) the third and fourth the He-, and CO_2- permeability of BS_1 respectively, the fifth and sixth columns the He-, and CO_2 permeability of Z_2, and the last two columns shows the He-, and CO_2 permeability of CC_3

Confining pressure (MPa)	Inlet pressure (MPa)	BS_1		Z_2		CC_3	
		k_{He} (m^2)	k_{CO2} (m^2)	k_{He} (m^2)	k_{CO2} (m^2)	k_{He} (m^2)	k_{CO2} (m^2)
10	4.5±0.2	3,61E-19	4,51E-20	1,01E-18	8,3E-19	7,5E-20	No flow
20	4.5±0.2	3,15E-19	2,49E-20	5,32E-19	2,6E-19	3,2E-20	No flow
30	4.5±0.2	3,13E-19	1,43E-20	3,97E-19	1,4E-19	5,8E-21	No flow

follow a positive correlation, as well as with the measurements of Febbo et al. (2025), since the first order of control on permeability is the pore-throat size and not the porosity, especially in nanoporous rocks (Xiao et al. 2017). This lack of correlation cannot be explained by the fractured samples, because the given permeability was recorded on the first day on an undisturbed sample.

The highest variability in porosity-permeability can be seen among the casing-cement samples having different compositions. CC_1 has the highest permeability, but the lowest porosity. The high permeability is due to a macroscopic fracture (red arrow, Fig. 2). On the other hand, the other casing cement samples contain polymer, which might reduce the gas permeability (Tsvigu et al. 2015) and porosity. Styrene-butadiene (SB) has good water resistance and fair gas permeability (Wen et al. 2020), while styrene-acrylic ester (SAE) has really good water resistance and can reduce the permeability (Dou et al. 2019). Ethylene vinyl acetate (EVA) has a high permeability to water vapor and gases, but is low permeability to oil and gas (Cooper 2013). However, this does not align with our results, where the cements containing this type of polymer were either impermeable or at the lower measurement limit. Therefore, based on our measurements, the styrene-butadiene (SB) and ethylene vinyl acetate (EVA) polymers might be the best for casing cement based on the limited number of samples.

Stress-dependent permeability

Permeability decreases with increasing confining stresses (Fig. 6) due to mechanical compaction, but different samples show different stress sensitivities. This can be linked to lithology and was also reported in previous studies (Chen et al. 2002; Ingebritsen and Manning 1999; Kozhevnikov et al. 2021). David et al. (1994) calculated the pressure sensitivity of permeability (γ-values) documented a relation

between the sensitivity coefficients and lithology. According to David et al. (1994), porous and permeable clastic rocks have $\gamma < 0.02$ MPa^{-1} as the upper boundary, with a pressure sensitivity coefficient γ of 0.02 MPa^{-1} as the lower boundary for tight rocks. The general correlation between different lithotypes can be established again (Fig. 4), with anhydrites and casing cements showing higher γ-values than claystones, tight sandstones and carbonates. In David et al. (1994) the γ -values of sandstones with high porosity lie in the range between 0.0066 and 0.012, and according to Yale and Nur (1984), tight sandstones range between 0.038 and 0.063. Samples BS_1, UC_5 and UC_6 fall in the range measured by David et al. (1994), while having slightly higher porosity than the reference samples, but still classifying as low-porous rock types. All other shale and sandstone samples fall into the range derived by Yale and Nur (1984), except for sample BS_2. According to Kilmer et al. (1987) and Monsees et al. (2020), the pressure sensitivity coefficient tends to increase with increasing depth and decreasing permeability. The difference in γ-value between sample BS_1 and BS_2 can be explained by different initial depths and the slight difference in permeability. This applies not only to the red claystone samples, but also to the anhydrite, and sandstone samples, where the samples with lower permeability came from greater depth.

In low porosity rocks ($\Phi < 5\%$), hydrostatic compaction is nonlinear and reversible. Therefore, the general assumption might not be applicable to some of these samples, e.g. anhydrite, black shale, one casing cement and one of the sandstones (David et al. 1994). The much lower γ-value of CC_4 compared to the other cement samples might be explained by the different types of polymer since EVA-polymer is not as sensitive to different strain rates (Ercan and Korkmaz 2021).

Jones (1980) observed that the cubic root of the permeability is linear to the logarithm of the confining pressure. Our results correspond to this equation; however, sample Cr_1 shows an increasing trend (Fig. 6a). The reason for that might be the general harder carbonate minerals (dolomite, calcite) than clay minerals, which cannot easily deform in a ductile manner (Guglielmi 2025). Hence, microcracks might have been developed during confining stress exposure in the sample, causing a permeability increase in the sample with increasing confining pressure, as Zhang et al. (2020) detected as well.

Time-dependent permeability

To understand the effect of permeability changes with time, which may be of importance during injection and the associated pressure increase, time dependent permeability measurements were carried out (Teklu et al. 2016). Eight samples were studied that experienced a confining pressure of 30 MPa for a week. They show a great variance in permeability over time until reproducible permeability values were achieved. In our measurements, helium was used as a permeant. The cause of the time-dependent permeability change is most likely compaction, mechanical creep or in case of permeability increase, cracking (Bandara et al. 2021; Chen et al. 2022; Zhu et al. 2024). The permeability of anhydrite samples decreases and stabilizes after 2–3 days, while the permeability of the red claystone converges after 4 days (Fig. 8). The black shale (UC_2) shows a sharp increase on the fifth day. This might be caused by the cracking of the sample as it was retrieved from the measurement setup containing an opened-up fracture (Fig. 2). Variation can be seen in the Cr_1 sample, where, in addition to the microcracks, calcisphere might have an influence on permeability. This carbonate sample contains 30% calcispheres and it does not show optical porosity, but the intragranular microporosity might be still high (Ölmez et al. 2024). This intragranular porosity might have compacted due to the elevated confining pressure, and afterwards the higher pore pressure caused again an increase in permeability. As the casing cement also shows increased permeability after 3 days, microfracturing due to continuous drying of the sample is likely, however only drying could increase permeability, due to particle shrinkage (He et al. 2017a, b). According to Chen et al. (2012) and Zhang et al. (2022) the gas permeability of cement increases with decreasing water saturation, which would be an alternative to explain permeability increase in cement samples, as our measurements were performed with dry gases. In addition, UC_5, UC_6, and Z_3 samples did not show a remarkable change in the permeability over time. This agrees with the higher initial permeability values. Based on this observation, we are able to conclude that there is a correlation between the γ-value and time (Fig. 8b), which is needed to achieve constant permeability values. Generally, samples having lower γ–values should take less time to achieve reproducible measurements (Fig. 8b). These observations support the assumption, that the rate of permeability change is influenced by the lithology and their respective ranges of stress sensitivity. A similar phenomenon was observed by Zhu et al. (2024), who stated that the rapid decline stage lasts up to 4–5 days. However, their samples were exposed to 10 MPa confining pressure, which may cause a longer rapid decline stage.

Hysteresis

For the stress hysteresis measurements, four loading-unloading cycles were carried out in 8 days. During the last cycle (day 8), the permeability increased during the unloading stage but with irreversible reduction in comparison to

Table 2 Mean free path of CO_2 and Helium at 4.5 MPa pressure

Pressure (MPa)	CO_2 (nm)	Helium (nm)
4.5	1.9	3.0

the initial value (Fig. 9). According to Chen et al.(2018), the permeability increase happens during the unloading period when the volumetric strain becomes negative, therefore instead of volumetric compression, volumetric expansion takes place. The expansion during unloading stage can lead to the growth of microfractures which are affecting permeability. This does not occur in the earlier unloading stages because viscoelastic deformation is time-dependent, and the initial compaction change is minimal during the early phases. Consequently, the strain release is insufficient to induce microfracture propagation, and therefore, the γ-values became higher. A similar phenomenon was observed by Zhang et al. (2020). The 3rd loading stage (Fig. 9, solid blue line) has higher permeability values at 20 and 30 MPa confining pressure than at 10 MPa. This is related to the gas flow, that has not reached steady-state conditions. The loading-unloading stages also affected the γ-values, which on the first loading day is the highest, 0.009 MPa^{-1}, then it stabilizes at around 0.005 MPa^{-1}. In the first cycle, the γ-value is higher during the loading stage than during the unloading stage, as the sample was previously unconfined, a reason why typically stress dependency permeability measurements should be performed during the stress-release path.

Gas-dependent permeability

Although permeability should not depend on the type of permeant gas (Civan 2010; Civan et al. 2011), CO_2 permeability was lower than helium permeability in both, BS_1 and Z_2 cases (Table 1) and in the casing cement the CO_2-permeability was not even measurable (lower than 10^{-22} m^2). Pore throat size measurements using MICP confirm the small pore throat sizes of the studied samples (Fig. 5), implying that Knudsen flow, rather than slip flow is occurring in the samples (Busch et al. 2017). This is supported by the calculated Knudsen numbers, that can be derived by the mean free path of the given gas (Table 2) and by the median pore throat size (Knudsen 1909; Orlander et al. 2021). The Knudsen numbers vary between 0.1 and 1 for BS_1 and Z_2, that suggest no slip flow, but Knudsen (transition) flow takes place (Knudsen 1909; Orlander et al. 2021). Therefore, Klinkenberg-correction is not applicable. Comparing just the apparent permeabilities however, highlight that at the same mean pressures, permeability of every rock toward CO_2 is lower than toward helium (Table 1).

This is in agreement with measurements by Gensterblum et al. (2014) and Tang et al. (2005) who measured permeability with different gases, including argon, methane, and CO_2 (Table 3). Gensterblum et al. (2014) found that permeability measured with helium is always higher than argon-, methane-, and nitrogen-permeability, while CO_2-permeability is always the lowest (Table 3). Gensterblum et al. (2014) and He et al. (2017a, b) relate these differences to molecule sizes of helium and CO_2. Based on Breck's kinetic diameters (Breck 1974), CO_2 molecules are larger (3.3 Å) than helium atoms (2.6 Å). A similar phenomenon was observed by Ghanizadeh et al. (2014a, b), although they did not use CO_2 as a permeant, but argon (3.4 Å) and methane (3.8 Å). In their measurement methane-permeability was always the lowest compared to other gases, which might be due to its highest kinematic diameter. However, based on the kinematic diameter, methane (3.8 Å) should have lower permeability than CO_2 (3.3 Å), but the opposite has be seen by Gensterblum et al. (2014). Based on the mean free paths of helium and carbon-dioxide, helium has longer mean free paths than carbon-dioxide, meaning the apparent He-permeability should be higher than of CO_2.

Furthermore, according to Ottiger et al. (2008), CO_2 adsorbs better on coal than methane, and Gensterblum et al. (2014) measured the gas-permeability on subbituminous coal. Therefore, the gas permeability also depends on the sorption of the gas as well (Jin and Firoozabadi 2013, 2014), especially, if the studied samples contain organic material.

Table 3 Comparison of permeability measured with different gases in previous studies. The first column displays the study, the second the lithology of the samples, the third the permeant and the fourth shows which gas had the highest permeability in each study

Publication	Lithology	Permeant gases	Comparison of gas permeability
This study	Anhydrite Casing cement Red shale	Carbon dioxide (CO_2) Helium (He)	$He >> CO_2$
Tang et al. (2005)	Porous media not defined	Carbon dioxide (CO_2) Helium (He) Hydrogen (H_2) Nitrogen (N_2)	$He >> H_2 >> N_2 >> CO_2$
Sinha et al. (2013)	Intact shale	Argon (Ar) Helium (He) Methane (CH_4)	$He >> Ar > CH_4$
Gensterblum et al. (2014)	subbituminous coal	Argon (Ar) Carbon dioxide (CO_2) Helium (He) Methane Nitrogen (N_2)	$He >> Ar \geq N_2 > CH_4 >> CO_2$
Ghanizadeh et al. (2014a, b)	Scandinavian Alum Shale	Argon (Ar) Helium (He) Methane (CH_4)	$He >> Ar > CH_4$
Ghanizadeh et al. (2014a, b)	Posidonia Shale	Argon (Ar) Helium (He) Methane (CH_4)	$He >> Ar > CH_4$

The BS samples contain predominantly hematite stained clay minerals forming the sample`s matrix (Figure S3, in supplementary materials). The clay minerals are chiefly composed of illite, based on characteristic interference colors. The cation exchange in clay minerals can increase the sorption of CO_2 (Jin and Firoozabadi 2013). Adsorption on illite can happen, but compared to montmorillonite, the amount of adsorbed CO_2 is much less (Jeon et al. 2014). Furthermore, Sinha et al. (2013) explains the much higher helium permeability with sorption as well, since helium is a non-sorbing gas, while CO_2 is a sorbing gas. However, sorption in anhydrite can happen only if the samples contain brine (Hangx et al. 2010; Isah et al. 2024). Since the samples were dry, sorption in anhydrite likely did not play an important role. This observation might simplify the permeability studies for CO_2-reservoir caprocks and implies that previously derived permeability measurements using non-CO_2 gases represent maximum permeabilities for possible sealing lithologies, as lower permeability values can be expected for CO_2 than for He. If a lithology is considered to be sealing in respect to helium it will also be considered sealing in respect to CO_2, given that no reactions are resulting from the lowered pH.

The casing cement samples might have contained some residual moisture, where the CO_2 could dissolve. Under the experimental pressure conditions, reactions might have happened between the solution and the portlandite, which leads to a reduction in permeability of the cement (Gan et al. 2025; Wang et al. 2020). However, this effect is interpreted as minimal, as continuous drying of casing cement samples likely leads to microfracturing and increases in permeability in casing cement samples using dry gases.

Sealing integrity

Insufficient sealing-integrity can lead to leakage, which is commonly due to too thin or too permeable caprocks (Bruno et al. 2014; Evans 2009). Purely based on our permeability measurements, the samples UC_5 (sandstone) and Z_3 (anhydrite) would not be considered as suitable caprocks, since the recommended permeability of a caprock should be lower than 10^{-18} m^2 (Chadwick et al. 2008; Falus et al. 2026). Although some of the rock samples (UC_2, UC_6, and Cr_1) show an increase or shifting trend in their permeability over time, the permeability still stays below 10^{-18} m^2 at 30 MPa confining stress, therefore, they are still suitable as possible seals. However, it is important to notice, that among the same rock formations there could be several orders of magnitude differences in the permeability values, therefore, defining suitable seals based only on the lithology, is not advisable. However, taking into account the artificial fracturing, sample UC_2 might be risky to use as a caprock due to the possible fracture development caused by stress change.

Casing cement provides an important barrier to prevent leakage. As Fig. 8 shows, under dry conditions and constant loading the casing cement shows a constant increase in permeability. Therefore, to avoid any leakage along the borehole, it is important to keep the cement water-saturated.

The permeability measurements were carried out at room temperature, where CO_2 is still in its gaseous phase, and no geochemical reactions were studied. However, He-permeability already gives a good indication, which rocktypes are impermeable enough to use as caprocks, since CO_2-permeability is always lower than He-permeability. Helium measurements could be preferred over CO_2 measurements, due to their safety, since helium is an inert noble gas and non-flammable. However, it is important to notice, that due to the dry CO_2 gas no chemical reactions happen. When injecting CO_2 into brine, processes of precipitation and dissolution have to be considered (Luquot and Gouze 2009). This especially affects the carbonate rocks and grains, where CO_2 can easily dissolve the minerals, likely increasing the permeability (Luquot and Gouze 2009). In addition, faults and fractures play an important role on sealing integrity (Bruno et al. 2014; Evans 2009).

Conclusions

All samples have porosities below 14% and permeability in the range of $1 \times 10^{-16} - 1 \times 10^{-22}$ m^2 at 30 MPa confining pressure. Permeability response to changing confining stress varies by lithology. The calculated mean γ-values for claystone, tight silty sandstones, and carbonate are below 0.02 MPa^{-1}, while casing cement and anhydrite have greater mean values than 0.02 MPa^{-1}. Claystones show the large variation in their γ-values compared to other sealing lithologies. Permeability, depth, and γ-values are correlated, lower permeability corresponds to higher γ-values. Stress-dependent permeability also relates to equilibration time. Samples with $\gamma < 0.02$ MPa^{-1} stabilize immediately, while those with $\gamma > 0.02$ MPa^{-1} require more than 3 days. Hysteresis measurements indicate permeability does not fully recover after pressure cycling, with γ-values higher during unloading stages than loading stages, likely due to microcrack development. Measured CO_2-permeabilities are consistently lower than He-permeabilities, reflecting gas-dependent effects from gas sorption and mostly from kinematic diameters. This gas-dependency is independent of lithology, implying that helium-based measurements represent maximum permeability, while actual permeability to CO_2 is always lower, due to the length of mean free path. This study indicates, that due to the heterogeneity of lithologies, site-specific assessment is required to define caprocks.

Supplementary Information The online version contains supplementary material available at https://doi.org/10.1007/s12665-026-12935-z.

Acknowledgements DJ thankfully acknowledges scholarship funding by Deutsche Bundesstiftung Umwelt – Central and Eastern Europe (DBU-CEE) Fellowship and KLIREC. The authors thank Martin von Dollen for thin section preparation, Sebastian Bruckschlögl for providing the casing cement samples, Andreas Bogner for MICP measurements, and Jasemin A. Ölmez for assistance during the measurements.

Authors' contributions DJ: Formal analysis, Methodology, Investigation, Validation, Visualization, Writing-original draft; BB: Conceptualization, Methodology, Investigation, Supervision, Writing – review and editing; CC: Resources, Writing – review and editing; CH: Supervision, Writing – review and editing.

Funding Open Access funding enabled and organized by Projekt DEAL.

Data availability No datasets were generated or analysed during the current study.

Declarations

Competing interests The authors declare no competing interests.

References

Abraham-A RM, Canas SSM, Miranda IF, Tassinari CC (2024) Assessment of CO_2 storage prospect based on physical properties of Rio Bonito Formation rock units. Energy Geoscience 5(1):100163

Alam AKMB, Niioka M, Fujii Y, Fukuda D, Kodama J-i (2014) Effects of confining pressure on the permeability of three rock types under compression. Int J Rock Mech Min Sci 65:49–61. https://doi.org/10.1016/j.ijrmms.2013.11.006

Alcalde J, Flude S, Wilkinson M, Johnson G, Edlmann K, Bond CE, Scott V, Gilfillan SMV, Ogaya X, Haszeldine RS (2018) Estimating geological CO_2 storage security to deliver on climate mitigation. Nat Commun 9(1):2201. https://doi.org/10.1038/s41467-018-04423-1

Atef H, Bossennec C, van der Vaart J, Sass I (2025) Structural assessment of the Belayim formation for future potential CO_2 storage, Gulf of Suez, Egypt. Geoenergy Sci Eng 252:213921. https://doi.org/10.1016/j.geoen.2025.213921

Bandara KMAS, Ranjith PG, Haque A, Wanniarachchi WAM, Zheng W, Rathnaweera TD (2021) An experimental investigation of the effect of long-term, time-dependent proppant embedment on fracture permeability and fracture aperture reduction. Int J Rock Mech Min Sci 144:104813. https://doi.org/10.1016/j.ijrmms.2021.104813

Becker I, Busch B, Koehrer B, Adelmann D, Hilgers C (2019) Reservoir quality evolution of Upper Carboniferous (Westphalian) tight gas sandstones, Lower Saxony Basin, NW Germany. J Pet Geol 42(4):371–392

Bernabé Y, Mok U, Evans B (2003) Permeability-porosity Relationships in Rocks Subjected to Various Evolution Processes. Pure appl Geophys 160(5):937–960. https://doi.org/10.1007/PL00012574

Boigk H (1959) *Zur Gliederung und Fazies des Bundsandsteins zwischen Harz und Emsland*

Breck DW (1974) Zeolite molecular sieves: structure, chemistry, and use. John Wiley & Sons, Inc., New York

Bruckschlögl S, Cheng C, Thissen P, Busch B, Hilgers C, Dehn F (2026) Hydrogen reactivity with wellbore and polymer-modified cements: experimental insights for safe underground hydrogen storage. Int J Hydrog Energy 210. https://doi.org/10.1016/j.ijhydene.2026.153578

Bruno MS, Lao K, Diessl J, Childers B, Xiang J, White N, van der Veer E (2014) Development of improved caprock integrity analysis and risk assessment Techniques. Energy Procedia 63:4708–4744. https://doi.org/10.1016/j.egypro.2014.11.503

Budinis S, Krevor S, Dowell NM, Brandon N, Hawkes A (2018) An assessment of CCS costs, barriers and potential. Energy Strategy Reviews 22:61–81. https://doi.org/10.1016/j.esr.2018.08.003

Busch A, Schweinar K, Kampman N, Coorn A, Pipich V, Feoktystov A, Leu L, Amann-Hildenbrand A, Bertier P (2017) Determining the porosity of mudrocks using methodological pluralism. Geol Soc Lond Special Publications 454(1):15–38. https://doi.org/10.1144/sp454.1

Carcione JM, Gei D, Yu T, Ba J (2019) Effect of clay and mineralogy on permeability. Pure appl Geophys 176(6):2581–2594. https://doi.org/10.1007/s00024-019-02117-3

Chadwick A, Arts R, Bernstone C, May F, Thibeau S, Zweigel P (2008) Best practice for the storage of CO^2 in saline aquifers-observations and guidelines from the SACS and CO2STORE projects (Vol. 14). British Geological Survey

Chandler MA, Kocurek G, Goggin DJ, Lake LW (1989) Effects ofStratigraphic Heterogeneity on Permeability in Eolian Sandstone Sequence, PageSandstone, Northern Arizona. AAPG Bulletin 73(5), 658-668.https://doi.org/10.1306/44b4a249-170a-11d7-8645000102c1865d

Chen Q, Kinzelbach W, Ye C, Yue Y (2002) Variations of Permeability and Pore Size Distribution of Porous Media with Pressure. J Environ Qual 31(2):500–505. https://doi.org/10.2134/jeq2002.5000

Chen W, Liu J, Brue F, Skoczylas F, Davy CA, Bourbon X, Talandier J (2012) Water retention and gas relative permeability of two industrial concretes. Cem Concr Res 42(7):1001–1013. https://doi.org/10.1016/j.cemconres.2012.04.003

Chen X, Tang C-a, Yu J, Zhou J-f, Cai Y-y (2018) Experimental investigation on deformation characteristics and permeability evolution of rock under confining pressure unloading conditions. J Cent South Univ 25(8):1987–2001. https://doi.org/10.1007/s11771-018-3889-2

Chen X, Xie SY, Zhang W, Armand G, Shao JF (2022) Creep deformation and Gas permeability in fractured claystone under various stress states. Rock Mech Rock Eng 55(4):1843–1853. https://doi.org/10.1007/s00603-022-02774-2

Civan F (2010) Effective Correlation of Apparent Gas Permeability in Tight Porous Media. Transp Porous Media 82(2):375–384. https://doi.org/10.1007/s11242-009-9432-z

Civan F, Rai CS, Sondergeld CH (2011) Shale-gas permeability and diffusivity inferred by Improved formulation of relevant retention and transport mechanisms. Transp Porous Media 86(3):925–944. https://doi.org/10.1007/s11242-010-9665-x

Cooper TA (2013) 4 - Developments in plastic materials and recycling systems for packaging food, beverages and other fast-moving consumer goods. In N. Farmer (Ed.), *Trends in Packaging of Food, Beverages and Other Fast-Moving Consumer Goods (FMCG)* (pp. 58–107). Woodhead Publishing. https://doi.org/10.1533/9780857098979.58

David C, Wong T-F, Zhu W, Zhang J (1994) Laboratory measurement of compaction-induced permeability change in porous rocks: Implications for the generation and maintenance of pore pressure excess in the crust. Pure appl Geophys 143(1):425–456. https://doi.org/10.1007/BF00874337

Dong J-J, Hsu J-Y, Wu W-J, Shimamoto T, Hung J-H, Yeh E-C, Wu Y-H, Sone H (2010) Stress-dependence of the permeability and porosity of sandstone and shale from TCDP Hole-A. Int J Rock Mech Min Sci 47(7):1141–1157. https://doi.org/10.1016/j.ijrmms.2010.06.019

Doornenbal H, Stevenson A (2010) *Petroleum Geological Atlas of the Southern Permian Basin Area* (H. Doornenbal & A. Stevenson, Eds.)

Dou J, Zhang G, Li S, Tian C, Ji C, Zhang C (2019) Properties of degraded waste PET-modified styrene-acrylic emulsions for cement slurry materials. Adv Civil Eng 2019(1):4624907. https://doi.org/10.1155/2019/4624907

Drozdzewski G (1993) The Ruhr coal basin (Germany): structural evolution of an autochthonous foreland basin. Int J Coal Geol 23(1):231–250. https://doi.org/10.1016/0166-5162(93)90050-K

Ecay L, Grégoire D, Pijaudier-Cabot G (2020) On the prediction of permeability and relative permeability from pore size distributions. Cem Concr Res 133. https://doi.org/10.1016/j.cemconres.2020.106074

Ercan N, Korkmaz E (2021) Structural, thermal, mechanical and viscoelastic properties of ethylene vinyl acetate (EVA)/olefin block copolymer (OBC) blends. Mater Today Commun 28:102634. https://doi.org/10.1016/j.mtcomm.2021.102634

Evans DJ (2009) A review of underground fuel storage events and putting risk into perspective with other areas of the energy supply chain. Geol Soc Lond Special Publications 313(1):173–216. https://doi.org/10.1144/SP313.12

Falus G, Cseresznyés D, Szamosfalvi Á, Szabó-Krausz Z, Szabó C, Király C (2026) Geological storage of CO_2 in Hungary: the overview of storage potential and the role of natural occurrences. Geol Soc Lond Special Publications 555(1):SP555. https://doi.org/10.1144/SP555-2023-196. -2023-2196

Febbo MB, Förster A, David W, Springer N, Norden B, Förster H-J (2025) The Upper Triassic caprock of the Ketzin CO_2 storage site, North German Basin: Implications for geological hydrogen storage. Geoenergy Sci Eng 253:213987. https://doi.org/10.1016/j.geoen.2025.213987

Filomena CM, Stollhofen H (2011) Ultrasonic logging across unconformities — outcrop and core logger sonic patterns of the Early Triassic Middle Buntsandstein Hardegsen unconformity, southern Germany. Sed Geol 236(3):185–196. https://doi.org/10.1016/j.sedgeo.2011.01.005

Friedlingstein P, O'Sullivan M, Jones MW, Andrew RM, Bakker DCE, Hauck J, Landschützer P, Quéré L, Luijkx C, Peters IT, Peters GP, Pongratz W, Schwingshackl J, Sitch C, Canadell S, Ciais JG, Jackson P, Alin RB, Anthoni SR, Zheng P, B (2023) Global Carbon Budget 2023. Earth Syst Sci Data 15(12):5301–5369. https://doi.org/10.5194/essd-15-5301-2023

Friedlingstein P, O'Sullivan M, Jones MW, Andrew RM, Hauck J, Landschützer P, Le Quéré C, Li H, Luijkx IT, Olsen A, Peters GP, Peters W, Pongratz J, Schwingshackl C, Sitch S, Canadell JG, Ciais P, Jackson RB, Alin SR, Zeng J (2025) Global Carbon Budget 2024. Earth Syst Sci Data 17(3):965–1039. https://doi.org/10.5194/essd-17-965-2025

Gan M, Hakuzweyezu T, Zhang L, Wang Y, Qin Q, Mei K, Cheng X (2025) Performance characterization of wellbore cement containing different CO_2-resisting additives under geologic CO_2 storage conditions. Geoenergy Sci Eng 245:213510. https://doi.org/10.1016/j.geoen.2024.213510

Geluk MC, Röhling HG (1997) High-resolution sequence stratigraphy of the Lower Triassic 'Buntsandstein' in the Netherlands and northwestern Germany. Geol Mijnbouw 76(3):227–246. https://doi.org/10.1023/A:1003062521373

Gensterblum Y, Ghanizadeh A, Krooss BM (2014) Gas permeability measurements on Australian subbituminous coals: fluid dynamic and poroelastic aspects. J Nat Gas Sci Eng 19:202–214

Ghanizadeh A, Amann-Hildenbrand A, Gasparik M, Gensterblum Y, Krooss BM, Littke R (2014a) Experimental study of fluid transport processes in the matrix system of the European organic-rich shales: II. Posidonia Shale (Lower Toarcian, northern Germany). Int J Coal Geol 123:20–33. https://doi.org/10.1016/j.coal.2013.06.009

Ghanizadeh A, Gasparik M, Amann-Hildenbrand A, Gensterblum Y, Krooss BM (2014b) Experimental study of fluid transport processes in the matrix system of the European organic-rich shales: I. Scandinavian Alum Shale. Mar Pet Geol 51:79–99. https://doi.org/10.1016/j.marpetgeo.2013.10.013

Giers R (1958) Die Mukronatenkreide im östlichen Münsterland

Greve J, Busch B, Quandt D, Knaak M, Hartkopf-Fröder C, Hilgers C (2023) Coupling heat conductivity and lithofacies of the coal-bearing Upper Carboniferous in the eastern Ruhr Basin, NW Germany. Z der Deutschen Gesellschaft für Geowissenschaften 4:673–695

Greve J, Busch B, Quandt D, Knaak M, Hilgers C (2024a) The influence of sedimentary facies, mineralogy, and diagenesis on reservoir properties of the coal-bearing Upper Carboniferous of NW Germany. Pet Geosci 30(1):petgeo2023–petgeo2020. https://doi.org/10.1144/petgeo2023-020

Greve J, Busch B, Quandt D, Knaak M, Hilgers C (2024b) Understanding the interplay of depositional rock types, mineralogy, and diagenesis on reservoir properties of the coal-bearing Langsettian and Duckmantian strata (Bashkirian, Pennsylvanian) of the Ruhr Area, NW Germany. Int J Earth Sci. https://doi.org/10.1007/s00531-024-02454-2

Guglielmi Y (2025) Influence of brittleness and ductility. In A Review of CO_2 Storage Integrity and Fault Zone Risk (pp. 15–31). Springer Nature Switzerland. https://doi.org/10.1007/978-3-031-81529-4_2

Hangx S, Spiers CJ, Peach CJ (2010) Mechanical behavior of anhydrite caprock and implications for CO_2 sealing capacity. J Geophys Research: Solid Earth 115(B7). https://doi.org/10.1029/2009JB006954

He Y, Cheng J, Dou X, Wang X (2017a) Research on shale gas transportation and apparent permeability in nanopores. J Nat Gas Sci Eng 38:450–457. https://doi.org/10.1016/j.jngse.2016.12.032

He Y, Cui Y-J, Ye W-M, Conil N (2017b) Effects of wetting-drying cycles on the air permeability of compacted Téguline clay. Eng Geol 228:173–179. https://doi.org/10.1016/j.enggeo.2017.08.015

Heap MJ (2019) The influence of sample geometry on the permeability of a porous sandstone. Geosci Instrum Method Data Syst 8(1):55–61. https://doi.org/10.5194/gi-8-55-2019

Hilgers C, Schilling FR (2024) Kohlendioxidabscheidung und geologische Speicherung (CCS)–ein Überblick. *Zeitschrift der Deutschen Gesellschaft für Geowissenschaften*

Ingebritsen SE, Manning CE (1999) Geological implications of a permeability-depth curve for the continental crust. Geology 27(12):1107–1110.

IPCC (2023) AR 6 synthesis report - Climate change (169 S.). https://www.ipcc.ch/report/ar6/syr

Isah A, Mahmoud M, Raza A, Murtaza M, Arif M, Kamal MS (2024) CO_2-brine interactions in anhydrite-rich rock: Implications for carbon mineralization and geo-storage. Int J Greenhouse Gas Control 137. https://doi.org/10.1016/j.ijggc.2024.104202

Jeon PR, Choi J, Yun TS, Lee C-H (2014) Sorption equilibrium and kinetics of CO_2 on clay minerals from subcritical to supercritical conditions: CO_2 sequestration at nanoscale interfaces. Chem Eng J 255:705–715. https://doi.org/10.1016/j.cej.2014.06.090

Jin Z, Firoozabadi A (2013) Methane and carbon dioxide adsorption in clay-like slit pores by Monte Carlo simulations. Fluid Phase Equilibria 360:456–465. https://doi.org/10.1016/j.fluid.2013.09.047

Jin Z, Firoozabadi A (2014) Effect of water on methane and carbon dioxide sorption in clay minerals by Monte Carlo simulations. Fluid Phase Equilibria 382:10–20. https://doi.org/10.1016/j.fluid.2014.07.035

Jones FO, Owens WW (1980) A laboratory study of low-permeability gas sands. J Petrol Technol 32(09):1631–1640. https://doi.org/10.2118/7551-pa

Kilmer NH, Morrow NR, Pitman JK (1987) Pressure sensitivity of low permeability sandstones. J Petrol Sci Eng 1(1):65–81. https://doi.org/10.1016/0920-4105(87)90015-5

Klinkenberg L (1941) The permeability of porous media to liquids and gases. Drill Prod Pract, 200–213

Knopp J, Steger H, Moormann C, Blum P (2022) Influence of weathering on pore size distribution of soft rocks. Geotech Geol Eng 40(11):5333–5346. https://doi.org/10.1007/s10706-022-02217-3

Knudsen M (1909) Die Gesetze der Molekularströmung und der inneren Reibungsströmung der Gase durch Röhren. Ann Phys 333(1):75–130. https://doi.org/10.1002/andp.19093330106

Kozhevnikov EV, Turbakov MS, Riabokon EP, Poplygin VV (2021) Effect of effective pressure on the permeability of rocks based on well testing results. *Energies*, *14*(8), 2306. https://www.mdpi.com/1996-1073/14/8/2306

Luquot L, Gouze P (2009) Experimental determination of porosity and permeability changes induced by injection of CO_2 into carbonate rocks. Chem Geol 265(1–2):148–159. https://doi.org/10.1016/j.chemgeo.2009.03.028

Massarweh O, Abushaikha AS (2024) CO_2 sequestration in subsurface geological formations: A review of trapping mechanisms and monitoring techniques. Earth Sci Rev, 104793

Menning M, Schröder B, Plein E, Simon T, Lepper J, Röhling H-G, Heunisch C, Stapf K, Lützner H, Käding K-C (2011) Beschlüsse der Deutschen Stratigraphischen Kommission 1991–2010 zu Perm und Trias von Mitteleuropa.[Recommendations of the German Stratigraphic Commission 1991–2010 on the Permian and Triassic of Central Europe]. Z der Deutschen Gesellschaft für Geowissenschaften 162(1):1–18

Meschede M (2018) Geologie Deutschlands: ein prozessorientierter Ansatz. Springer, Berlin, p 255

Molenaar N, Cyziene J, Sliaupa S (2007) Quartz cementation mechanisms and porosity variation in Baltic Cambrian sandstones. Sed Geol 195(3):135–159. https://doi.org/10.1016/j.sedgeo.2006.07.009

Monsees AC, Busch B, Schöner N, Hilgers C (2020) Rock typing of diagenetically induced heterogeneities – A case study from a deeply-buried clastic Rotliegend reservoir of the Northern German Basin. Mar Pet Geol 113:104163. https://doi.org/10.1016/j.marpetgeo.2019.104163

Muller A, Steingrobe B (1991) Sedimentologie der oberkarbonischen Schichtenfolge in der Forschungsbohrung Frenzer Staffel 1 (1985), Aachen-Erkelenzer Steinkohlenrevier-Deutung der vertikalen und lateralen Trendentwicklungen. Geol Jahrbuch Reihe Allgemeine und regionale Geologie BR Deutschland und Nachbargebiete Tektonik Stratigraphie Paläontologie 116:87–127

Neuzil CE (2019) Permeability of Clays and Shales. *Annual Review of Earth and Planetary Sciences*, *47*(Volume 47, 2019), 247–273. https://doi.org/10.1146/annurev-earth-053018-060437

Ölmez JA, Busch B, Hilgers C (2024) Reservoir quality of Upper Cretaceous limestones (Ahlen-Fm., Beckum Member, Münsterland Cretaceous Basin): effects of cementation and compaction on the compactable depositional volume. Int J Earth Sci. https://doi.org/10.1007/s00531-024-02411-z

Orlander T, Milsch H, Fabricius IL (2021) Comparison of gas, Klinkenberg, and liquid permeability of sandstone: Flow regime and pore size. AAPG Bull 105(7):1383–1403

Ottiger S, Pini R, Storti G, Mazzotti M (2008) Measuring and Modeling the Competitive Adsorption of CO_2, CH4, and N2 on a Dry Coal. Langmuir 24(17):9531–9540. https://doi.org/10.1021/la801350h

Quandt D, Rudolph T, Hilgers C (2022) Post-Mining: Geomonitoring, process understanding, and utilisation of former mining areas. J Appl Reg Geology/Zeitschrift der Deutschen Gesellschaft für Geowissenschaften (ZDGG), *173*(4)

Sander R, Pan Z, Connell LD (2017) Laboratory measurement of low permeability unconventional gas reservoir rocks: A review of experimental methods. J Nat Gas Sci Eng 37:248–279. https://doi.org/10.1016/j.jngse.2016.11.041

Schmidt C, Busch B, Hilgers C (2020) Lateral variations of detrital, authigenic and petrophysical propertiesin an outcrop analog of the fluvial Plattensandstein, Lower Triassic, Central Germany. Zeitschrift der Deutschen Geologischen Gesellschaft 172(4):541-564. https://doi.org/10.1127/zdgg/2020/0234

Scheck-Wenderoth M, Krzywiec P, Zühlke R, Maystrenko Y, Froitzheim N (2008) Permian to Cretaceous tectonics.

Sinha S, Braun EM, Determan MD, Passey QR, Leonardi SA, Boros JA, Wood AC, Zirkle T, Kudva RA (2013) Steady-state permeability measurements on intact shale samples at reservoir conditions - Effect of stress, temperature, pressure, and type of gas. SPE Middle East Oil and Gas Show and Conference

Strozyk F, Reuning L, Scheck-Wenderoth M, Tanner DC (2017) Chapter 10 - The Tectonic History of the Zechstein Basin in the Netherlands and Germany. In Soto JI, Flinch JF, Tari G (eds.) *Permo-Triassic Salt Provinces of Europe, North Africa and the Atlantic Margins* (pp. 221-241), Elsevier. https://doi.org/10.1016/B978-0-12-809417-4.00011-2

Szurlies M (2004) Magnetostratigraphy: the key to a global correlation of the classic Germanic Trias-case study Volpriehausen Formation (Middle Buntsandstein), Central Germany. Earth Planet Sci Lett 227(3):395–410. https://doi.org/10.1016/j.epsl.2004.09.011

Tang GH, Tao WQ, He YL (2005) Gas slippage effect on microscale porous flow using the lattice Boltzmann method. Phys Rev E 72(5):056301. https://doi.org/10.1103/PhysRevE.72.056301

Teklu TW, Zhou Z, Li X, Abass H (2016) Experimental investigation on permeability and porosity hysteresis in low-permeability formations. SPE Low Perm Symposium

Tsvigu C, Pavesi E, De Angelis MG, Giacinti Baschetti M (2015) Effect of relative humidity and temperature on the gas transport properties of 6FDA–6FpDA polyimide: Experimental study and modelling. J Membr Sci 485:60–68. https://doi.org/10.1016/j.memsci.2015.02.032

Voigt T, Kley J, Voigt S (2021) Dawn and dusk of Late Cretaceous basin inversion in central Europe. Solid Earth 12(6):1443–1471. https://doi.org/10.5194/se-12-1443-2021

Wang R, Yu J, Gu S, He P, Du W, Han X, Liu Q (2020) Influence of ion chelator and CO_2-rich environment on self-healing capabilities of cement-based materials. Constr Build Mater 259:119685. https://doi.org/10.1016/j.conbuildmat.2020.119685

Wen S, Zhang R, Xu Z, Zheng L, Liu L (2020) Effect of the topology of carbon-based nanofillers on the filler networks and gas barrier

properties of rubber composites. Materials 13(23):5416. https://www.mdpi.com/1996-1944/13/23/5416

Wong LNY, Li D, Liu G (2013) Experimental studies on permeability of intact and singly jointed meta-sedimentary rocks under confining pressure. Rock Mech Rock Eng 46(1):107–121. https://doi.org/10.1007/s00603-012-0251-0

Wrede V, Zeller M (1991) Die stratigraphische Einstufung der Bohrung Frenzer Staffel 1 (1985) (Inde-Mulde, Aachener Steinkohlenrevier). Geol Jahrbuch Reihe Allgemeine und regionale Geologie BR Deutschland und Nachbargebiete Tektonik Stratigraphie Paläontologie 116:73–86

Xiao D, Lu S, Yang J, Zhang L, Li B (2017) Classifying multiscale pores and investigating their relationship with porosity and permeability in tight sandstone gas reservoirs. Energy Fuels 31(9):9188–9200. https://doi.org/10.1021/acs.energyfuels.7b01487

Yale DP, Nur A (1984) Network modeling of flow, storage, and deformation in porous rocks. In *SEG Technical Program Expanded Abstracts 1985* (pp. 91–94). https://doi.org/10.1190/1.1892843

Yang X, Meng Y, Shi X, Li G (2017) Influence of porosity and permeability heterogeneity on liquid invasion in tight gas reservoirs. J Nat Gas Sci Eng 37:169–177. https://doi.org/10.1016/j.jngse.2016.11.046

Zhang Q, Liu J, Wang L, Luo M, Liu H, Xu H, Zou H (2020) Impurity effects on the mechanical properties and permeability characteristics of salt rock. *Energies*, *13*(6), 1366. https://www.mdpi.com/1996-1073/13/6/1366

Zhang Y, Fang L, Wu S, Du S, Zhang J (2022) Time dependency and similarity of gas permeability of concrete in simulated environment. J Building Eng 51:104253. https://doi.org/10.1016/j.jobe.2022.104253

Zhao X, Chen Z, Zhang L, Liao X, Awotunde AA (2024) Leakage risk assessment on sealing efficiency of caprock during CO_2 huff-n-puff for safe sequestration. Geoenergy Sci Eng 240:213056. https://doi.org/10.1016/j.geoen.2024.213056

Zhu N, Cheng P, Yu Q (2024) Experimental study on the time-dependent gas permeability of fractures in shales. Rock Mech Rock Eng 57(1):695–718. https://doi.org/10.1007/s00603-023-03578-8